Indian J Phys (January 2022) 96(1):267–274
https://doi.org/10.1007/s12648-020-01957-3

ORIGINAL PAPER

Influence of top layer on the linear and nonlinear optical parameters of Ag(Te)/$As_{50}Se_{50}$ bilayer thin films

D Sahoo[1], P Priyadarshini[1], D Alagarasan[2], R Ganesan[2], S Varadharajaperumal[3] and R Naik[1]*

[1]Department of Physics, ICT-IOC, Bhubaneswar 751013, India

[2]Department of Physics, Indian Institute of Science, Bangalore 560012, India

[3]Centre for Nano Science and Engineering, Indian Institute of Science, Bangalore 560012, India

Received: 30 January 2020 / Accepted: 23 October 2020 / Published online: 3 January 2021

Abstract: The present paper illustrates the influence of the top Ag and Te thin layer on the linear and nonlinear optical properties of Ag(Te)/$As_{50}Se_{50}$ bilayer thin films. The $As_{50}Se_{50}$ and Ag(Te)/$As_{50}Se_{50}$ bilayer thin films were prepared by thermal evaporation technique under high vacuum conditions. The X-ray diffraction study showed no structural changes, whereas the UV–Visible spectroscopy data showed the changes in optical properties due to top layer deposition. From the recorded optical transmission data, the optical parameters, such as absorption coefficient, extinction coefficient, optical bandgap, Tauc parameter, Urbach energy, linear refractive Index, oscillator energy, dispersion energy, high-frequency dielectric constant and carrier concentration, were evaluated. The transmittance decreased and the absorption coefficient increased along with the increase in extinction coefficient. The optical bandgap decreased due to the increase in defect states and the degree of disorder. The dispersion of the refractive index was analyzed by the single oscillator Wemple–Di Domenico model. The third-order nonlinear susceptibility ($\chi^{(3)}$) and nonlinear refractive index (n_2) were calculated from the linear optical parameters using semi-empirical relations. The linear, nonlinear refractive index and ($\chi^{(3)}$ change was found to be more in Te/$As_{50}Se_{50}$ film than that of Ag/$As_{50}Se_{50}$ film as compared with the host $As_{50}Se_{50}$ film. The surface morphology was investigated by field emission scanning electron microscopy. The tuning of optical properties by simple layer deposition on the host matrix can be used in various optoelectronic applications.

Keywords: Thin films; Optical properties; Refractive index; Bandgap; Nonlinear properties

1. Introduction

Chalcogenides are potential candidates in various technological applications, such as optoelectronics [1], IR fiber [2], memory devices [3] and xerography [4]. The high-quality multilayer and bilayer films of such amorphous semiconductors provide potential applications in the field of micro and optoelectronics. The chalcogenide multilayer films are an attractive system having many potential applications in various modern technologies. For example, the holographic gratings can be prepared from Ag/$As_{30}Se_{70}$ bilayer films [5], whereas Sb/As_2S_3 metal–chalcogenide layer can be used as an efficient media for the optical, amplitude-phase recording of patterns for optoelectronics [6]. The binary metal/chalcogenide compounds offer a lot of scope for various application-oriented studies due to their layered structure. The ternary Ag–Sb–S films are potential candidates for rewritable optical data storage applications which can be prepared from the heterogeneous structure of Ag/Sb_2S_3 with laser-induced or heat-induced effects as in other films, such as Te/$As_2Se_3$and Bi/As_2Se_3. [7, 8]. The family of Ag-doped chalcogenides includes interesting materials that focused on various studies such as the fabrication of photonic crystal waveguides from Ag/As_2Se_3 films [9] and tuning of optical bandgap by top layer Ag/Bi deposition onto Sb_2S_3 thin films [10]. Apart from the above discussed important applications based on their linear properties, the chalcogenide films possess high nonlinear behavior which makes them more efficient materials for application point of view. However, to build a useful device and estimate its potential performance, it is necessary to know its nonlinear properties. To design nonlinear optical devices, it is very important to examine nonlinear

*Corresponding author, E-mail: ramakanta.naik@gmail.com

optical properties, such as the third-order nonlinear susceptibility (χ^3), second-order nonlinear refractive index (n_2) and two-photon absorption coefficient (β_2). [11].

The third-order nonlinear optical effects in the infrared region allow for all-optical high-capacity communication networks, tunable mid-infrared light sources that are hard to reach by other means, remote sensing and medical diagnostics [12–14]. The key parameter to such applications is the availability of an appropriate nonlinear medium, and chalcogenide films with high conversion efficiencies are the best candidate at present time. As compared to silica, the chalcogenide films possess a high order of nonlinearity, approximately 100 times greater than that of silica [15]. High nonlinear refractive index along with moderate to low nonlinear absorption can be used in all-optical signal-processing devices to empower telecommunication systems [16]. The nonlinear constants, such as χ^3 and n_2, are utilized for the fabrication of optical waveguides, diffractive optical elements and micro-optical elements [17–19]. The nonlinear optical behavior of such films is of special interest due to their optical switching ability [20]. The parameter χ^3 which explains the third harmonic generation and two-photon absorption is an important parameter that decides the applicability of that material in the nonlinear optical device [21]. The 3rd order nonlinearity was enhanced by the doping of Ag atoms into alloys for suitable nonlinear applications [22]. So, it is desirable to form thin films that exhibit high nonlinear optical properties. There are several ways to make the desired film, but we have fabricated the bilayer films with high nonlinear values by deposition of Ag and Te layer onto $As_{50}Se_{50}$ film.

The aim of the present work was to investigate the effect of the Ag and Te top layer on the linear and nonlinear optical properties change in bilayer $Ag/As_{50}Se_{50}$ and $Te/As_{50}Se_{50}$ thin films as compared to the host $As_{50}Se_{50}$ film. The optical properties, including transmission, absorption, optical bandgap (E_g), linear refractive index (n), dispersion energy, oscillator energy, n_2, χ^3 etc., were determined from UV–Visible transmission spectra, and the nonlinear parameters were evaluated by the semiempirical formula. The structural investigation was carried out by X-ray diffraction (XRD) and the surface morphology was investigated from the field emission scanning electron microscopy (FESEM).

2. Experimental details

Thin films of $As_{50}Se_{50}$, $Ag/As_{50}Se_{50}$ and $Te/As_{50}Se_{50}$ were made from bulk $As_{50}Se_{50}$ (prepared by melt quenching method), Ag and Te (99.999% high purity elements from Aldrich and Sigma Chemical Company) by thermal evaporation method at a pressure of about 10^{-5} Torr. The films were deposited on glass substrates at 300 K, and the substrates were rotated slowly during the deposition process to obtain the homogenous and smooth film. The thickness of the thin film was 800 nm ($As_{50}Se_{50}$), 808 nm ($Ag/As_{50}Se_{50}$) and 808 nm ($Te/As_{50}Se_{50}$), respectively, which was measured by the crystal quartz monitor during the deposition process and the rate of deposition was 2 nm/s.

The structural information was obtained from XRD (Philips, CuK_α, = 1.54 Å). The XRD measurements were taken at 40 mA current and 40 kV voltage with a scan speed of 1° min^{-1}, a step value of 0.02° in 2θ range of 10° - 80° at a grazing angle of 1°. The surface morphology of the films was taken in FESEM (Sirion XL 40) with the scan at 20 kV with 40 μA emission current exposing a sample of 1 cm^2 size at 2×10^{-7} Torr pressure. The optical transmission spectra of the three films were taken by UV–Visible spectrometer (Bruker Optics (IFS66v/S) in the visible wavelength range 500–1200 nm. The measurement was done inside the sample chamber of the spectrometer in dark conditions. The linear optical quantities, such as absorption coefficient (α), optical bandgap (E_g), and Tauc parameter ($B^{1/2}$), were calculated from Tauc relation, whereas the Swanepoel method was used to calculate the linear refractive index. The dispersion parameters were obtained from a single oscillator Wemple–Di Domenico model. The nonlinear parameters, such as n_2 and χ^3, were evaluated by Miller's formula.

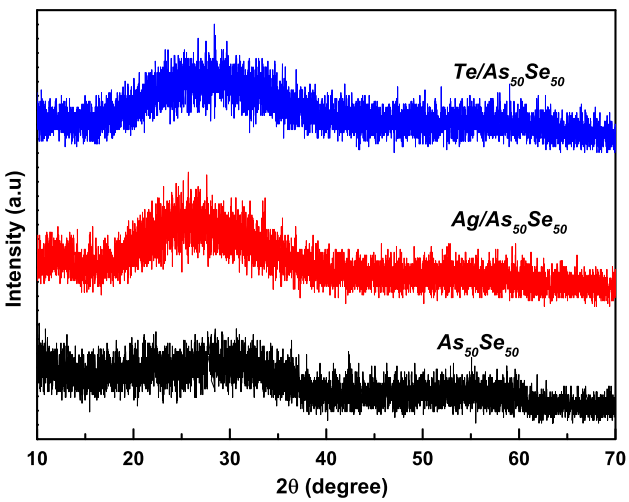

Fig. 1 XRD patterns of $As_{50}Se_{50}$, $Ag/As_{50}Se_{50}$ and $Te/As_{50}Se_{50}$ thin films

3. Results and discussion

3.1. Structural and surface morphology study

The XRD patterns of the studied thin films are presented in Fig. 1. The absence of any crystalline peaks and the presence of a broad hump confirms the amorphous nature of the prepared films. The three patterns look alike so that no differences can be noticed among the thin films. This infers that there is no structural change in the bilayer film due to Te and Ag deposition onto the $As_{50}Se_{50}$ host matrix.

However, the surface morphology change is visible in the FESEM images of $As_{50}Se_{50}$, $Ag/As_{50}Se_{50}$ and $Te/As_{50}Se_{50}$ thin films which are presented in Fig. 2. The surfaces of $As_{50}Se_{50}$ and $Te/As_{50}Se_{50}$ films are smooth and homogenous, whereas it is different in the case of $Ag/As_{50}Se_{50}$ film. The small agglomerate type structure is clearly noticed in the $Ag/As_{50}Se_{50}$ film and such wrinkle-like structure might be due to the Ag particles at the interface of the bilayer film. The wrinkle-like formations are interconnected with each other and do not have a particular orientation as found by also other studies [23]. The wrinkle-like formations are of various sizes as noticed and their length extends up to 2 μm.

3.2. Linear optical parameters

3.2.1. Transmission, absorption and extinction coefficient

The optical transmission spectra give necessary information about the band structure of the semiconducting materials and other useful parameters. The transmittance spectra as recorded for $As_{50}Se_{50}$, $Ag/As_{50}Se_{50}$ and $Te/As_{50}Se_{50}$ thin films in the wavelength () range 500–1200 nm are presented in Fig. 3. The nonshrinking interference fringes observed in the transmittance spectra at a higher wavelength (700–1200 nm) indicate the homogeneity and smoothness of the deposited films [24]. It has been observed that the transmission % decreased from 78% ($As_{50}Se_{50}$) to 64% for the $Ag/As_{50}Se_{50}$ film and 48% for

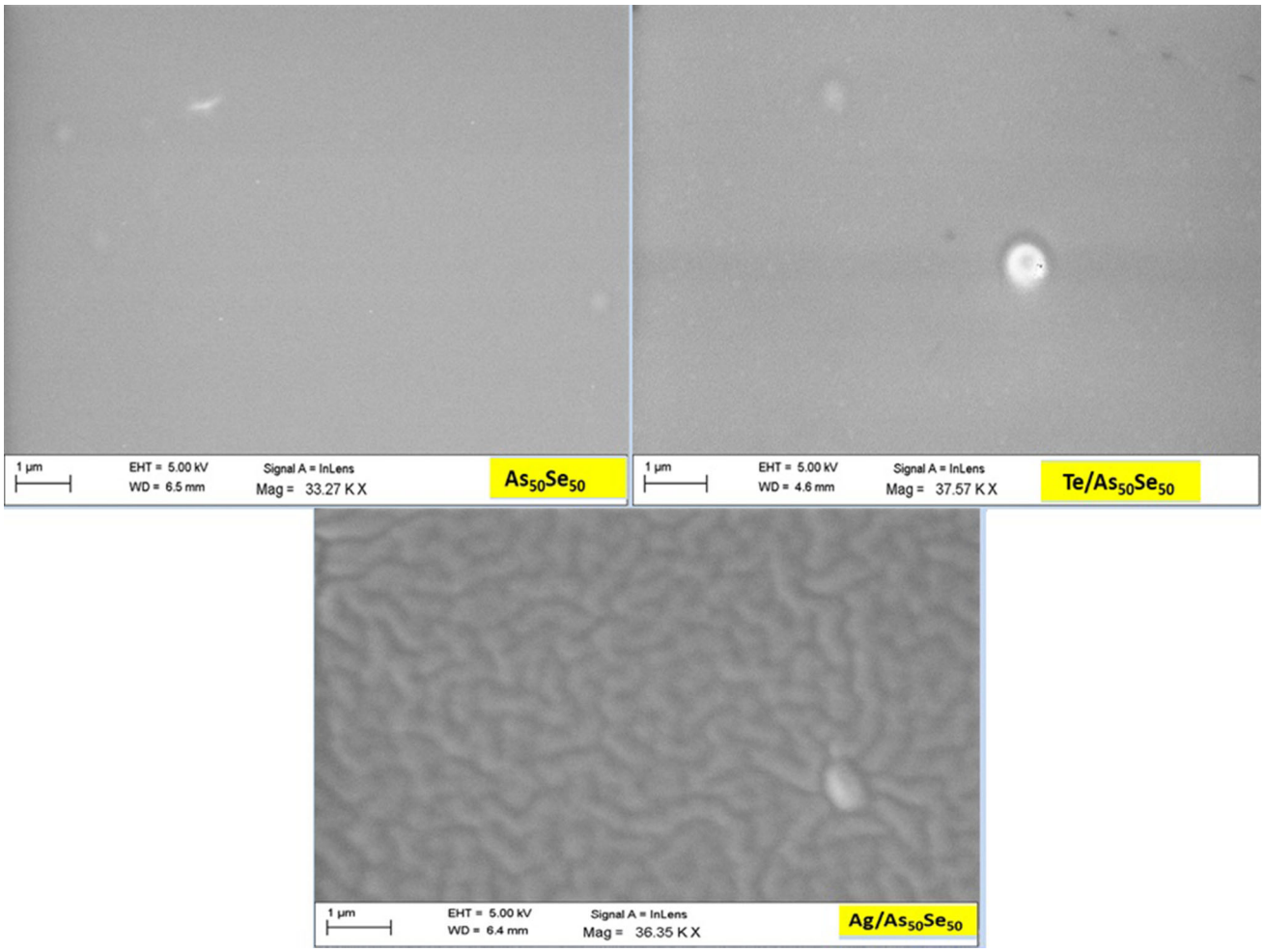

Fig. 2 FESEM images of $As_{50}Se_{50}$, $Ag/As_{50}Se_{50}$ and $Te/As_{50}Se_{50}$ thin films

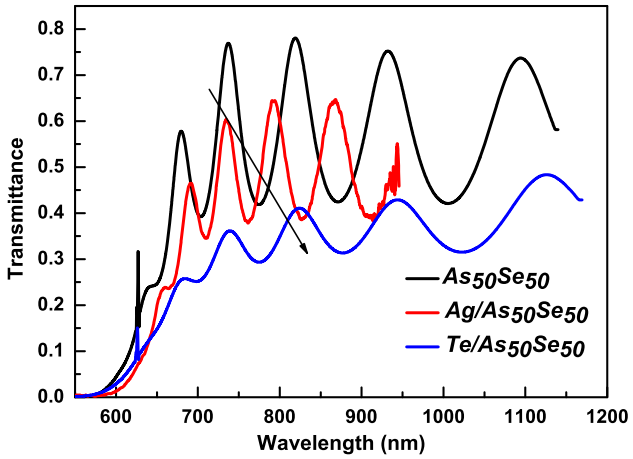

Fig. 3 Transmittance plot of $As_{50}Se_{50}$, $Ag/As_{50}Se_{50}$ and $Te/As_{50}Se_{50}$ thin films

the $Te/As_{50}Se_{50}$ thin film. We have shown the spectra for $Ag/As_{50}Se_{50}$ thin film up to 950 nm due to the appearance of noise after 950 nm. Furthermore, the absorption edge of the deposited films shows a shift which indicates the change of the optical bandgap for $Ag/As_{50}Se_{50}$ and $Te/As_{50}Se_{50}$ thin films.

The absorption coefficient in the strong absorption region was calculated by using the formula [25]

$$\alpha = \left(\frac{1}{d}\right) \ln\left(\frac{1}{T}\right), \tag{1}$$

where d is the thickness of the film, and T is the transmission of the films. The absorption coefficient is more for $Ag/As_{50}Se_{50}$ and $Te/As_{50}Se_{50}$ film than $As_{50}Se_{50}$ film as shown in Fig. 4.

The mass extinction coefficient (k) measures how strongly the film absorbs the light at a given which is related to the absorption coefficient and wavelength by [26].

$$k = \frac{\alpha\lambda}{4\pi} \tag{2}$$

The variation of k with is shown in Fig. 5 that depicts the increase in k value, with Te and Ag deposition onto $As_{50}Se_{50}$ thin film. However, the value is more for the Te deposited film than the Ag layer film. Since k is related to the surface defects and disorder parameter, it infers the increase in density of defect states leading to the decrease in E_g which is discussed in the following section.

3.2.2. *Optical bandgap (E_g), Tauc parameter ($B^{1/2}$) and Urbach energy (E_u)*

The fundamental absorption edge in most amorphous semiconductors follows an exponential law. In the high absorption region, the photon energy dependence of the absorption coefficient in allowed indirect transition can be described by Tauc's relation [27].

$$(\alpha h\vartheta)^{1/2} = B^{1/2}\left(h\vartheta - E_g\right), \tag{3}$$

where B is the Tauc parameter which depends on transition probability and measures the degree of disorder and E_g is the optical bandgap [27]. By plotting the linear portions of the dependence of $(\alpha h\upsilon)^{1/2}$ versus $h\upsilon$ will give a straight line and the X-intercept gives the optical bandgap as shown in Fig. 6. The slope of the fitting gives the degree of disorder value ($B^{1/2}$). The optical bandgap of $As_{50}Se_{50}$ was 1.71 ± 0.01 eV which decreased to 1.68 ± 0.01 eV for the $Ag/As_{50}Se_{50}$ film with Ag deposition. This decrease in E_g was due to the increase in density of localized states which reduced the optical bandgap. With the deposition of Te onto $As_{50}Se_{50}$, the E_g value was 1.60 ± 0.02 eV which is 0.08 eV less than that for $Ag/As_{50}Se_{50}$ film. This

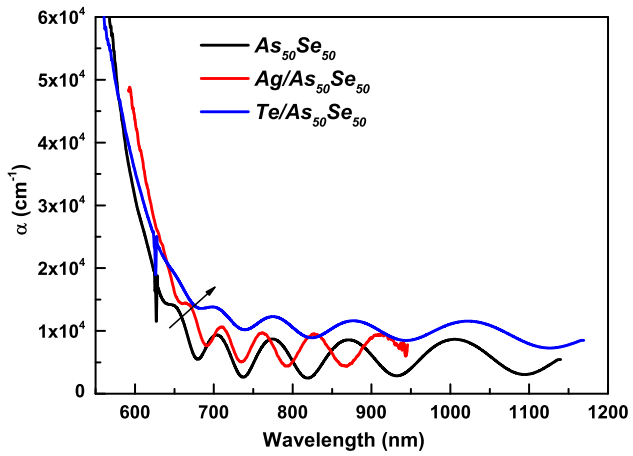

Fig. 4 α vs plot of $As_{50}Se_{50}$, $Ag/As_{50}Se_{50}$ and $Te/As_{50}Se_{50}$ thin films

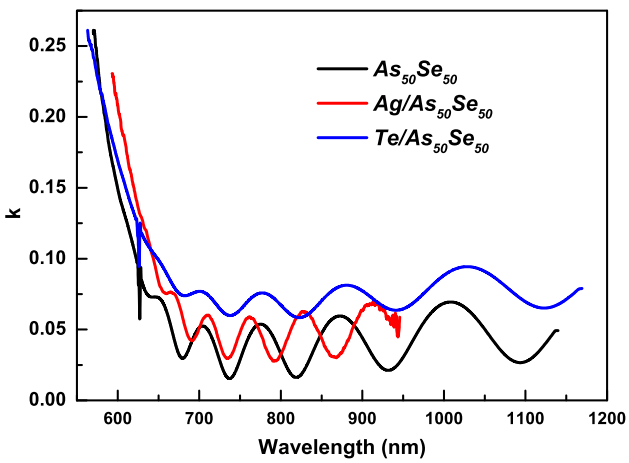

Fig. 5 Variation of k with of studied thin films

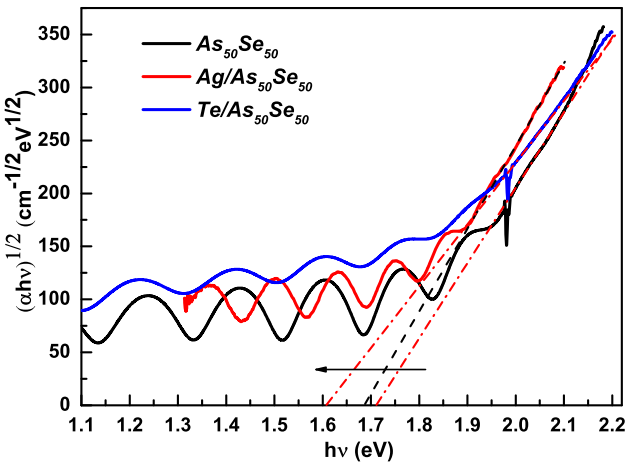

Fig. 6 $(\alpha h\nu)^{1/2}$ vs $h\nu$ for $As_{50}Se_{50}$, $Ag/As_{50}Se_{50}$ and $Te/As_{50}Se_{50}$ thin films

difference might be due to the less electronegativity of Ag (1.93) than Te (2.1) [28].

The decrease in E_g after Te and Ag deposition is well understood by the Mott and Davis model [29] which proposes that the number of defects and degree of disorder influences the width of the localized states near the mobility edge in an amorphous structure. The localized states have a strong influence on the optical absorption and thus on the optical bandgap. The deposition of Ag and Te onto $As_{50}Se_{50}$ film formed a greater number of homopolar bonds at the interface which enhanced the degree of disorder in the new bilayer films. Therefore, the magnitude of the density of defects increased which increased the width of the localized states, and consequently, the E_g value decreased for the bilayer films [26, 30].

The degree of disorder is noticed from the $B^{1/2}$ values which are 793 ± 3 $cm^{-1/2}$ $eV^{-1/2}$ ($As_{50}Se_{50}$), 759 ± 2 $cm^{-1/2}$ $eV^{-1/2}$ ($Ag/As_{50}Se_{50}$), and 698 ± 2 $cm^{-1/2}$ $eV^{-1/2}$ ($Te/As_{50}Se_{50}$), respectively, as shown in Table 1. The decrease in $B^{1/2}$ value infers the increase in disorder in the films due to more homopolar bond formation at the interface of the two layers. So, the degree of disorder is more in Te deposited film than that of Ag deposited film.

The width of the localized states E_u (Urbach energy) also measures the amount of disorder in a system. This parameter is being evaluated in the weak absorption region of the absorption spectrum from an exponential dependence on photon energy [31]

$$\alpha(h\nu) = \alpha_0 \exp\left(\frac{h\nu}{E_u}\right), \tag{4}$$

where ν is the frequency of the radiation, α_0 is a constant that corresponds to the absorption coefficient at bandgap, h is Planck's constant. The E_u value was calculated from the reciprocal of the slope of the linear portion of the dependence of ln (α/α_0) versus $h\nu$. The calculated E_u values for the as-deposited $As_{50}Se_{50}$, $Ag/As_{50}Se_{50}$and $Te/As_{50}Se_{50}$ thin films are presented in Table 1. The increased E_u values confirm the increase of disorder in the $Ag/As_{50}Se_{50}$ and $Te/As_{50}Se_{50}$ films. The greater value in the case of $Te/As_{50}Se_{50}$ film than $Ag/As_{50}Se_{50}$ one clearly showed more disorder in Te film than that of Ag film. The presented values of $B^{1/2}$ and E_u showed the inverse relation between them as studied in various other films [32, 33].

3.2.3. *Linear refractive Index (n), oscillator energy (E_o), dispersion energy (E_d)*

The linear refractive index was calculated from the transmission spectrum by using the Swanepoel method [34]. The required equation for the linear refractive index (n) is given by

$$n = \left[N + \left(N^2 - s^2\right)^{1/2}\right]^{1/2}, \tag{5}$$

where

$$N = 2s\left(\frac{T_M - T_m}{T_M T_m}\right) + \frac{s^2 + 1}{2} \tag{6}$$

T_M and T_m are the maxima and minima of the transmission curve at a particular wavelength; s is the refractive index of the glass substrate (1.51). The refractive index was found to be increased with Ag and Te deposition onto $As_{50}Se_{50}$ film as shown in Fig. 7 which is due to the increase of the number of unsaturated defects. These defects increased the density of localized states in the band structure thus increasing the refractive index. The red or blue shift of the bandgap values is related to the increase or decrease in the refractive index as stated by Moss's rule ($E_g n^4 \sim$ constant) as found in other studies [35, 36]. The change in 'n'

Table 1 Optical parameters of the studied films

Sample	Bandgap (E_g) in eV	$B^{1/2}$ in $cm^{-1/2}$ $eV^{-1/2}$	Urbach energy (meV)	E_0 (eV)	E_d (eV)	n_0
$As_{50}Se_{50}$	1.71±0.01	793±3	202±1	3.94	27.85	2.84
$Ag/As_{50}Se_{50}$	1.68±0.01	759±2	237±2	3.89	27.75	2.85
$Te/As_{50}Se_{50}$	1.60±0.02	698±2	284±2	3.99	30.32	2.93

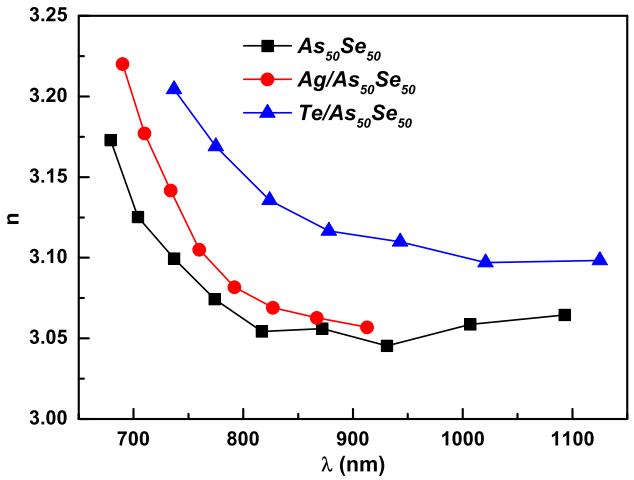

Fig. 7 n versus plot of $As_{50}Se_{50}$, $Ag/As_{50}Se_{50}$ and $Te/As_{50}Se_{50}$ thin films

value is more in $Te/As_{50}Se_{50}$ film than that of $Ag/As_{50}Se_{50}$ film.

The single effective oscillator model (Wemple and Di Domenico) for the dispersion of refractive index [37] is given by the formula

$$n^2(h\upsilon) = 1 + \frac{E_0 E_d}{E_0^2 - (h\upsilon)^2}, \tag{7}$$

where h is Planck's constant, E_o is the average excitation energy for electronic transition which is empirically related to the optical bandgap, while E_d is the dispersion energy that measures the average optical transition strength. The value of E_o and E_d was obtained from the slope $(E_o E_d)^{-1}$ and intercept (E_o/E_d) on the vertical axis (Fig. 8). The value of E_o for $As_{50}Se_{50}$, $Ag/As_{50}Se_{50}$ and $Te/As_{50}Se_{50}$ thin films are 3.94, 3.89 and 3.99 eV, respectively. Similarly, the E_d value for $As_{50}Se_{50}$, $Ag/As_{50}Se_{50}$ and $Te/As_{50}Se_{50}$ thin films are 27.85, 27.75 and 30.32 eV,

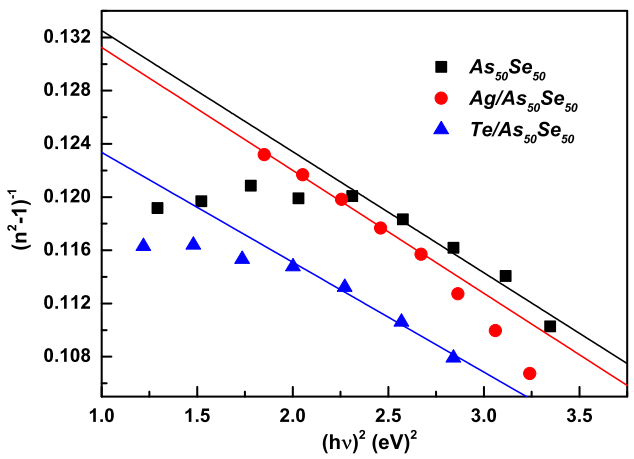

Fig. 8 $(n^2 - 1)^{-1}$ versus $(h\upsilon)^2$ plot of $As_{50}Se_{50}$, $Ag/As_{50}Se_{50}$ and $Te/As_{50}Se_{50}$ thin films

respectively. This variation is due to the variation of scattering centers. The static refractive index (n_0) was calculated from the relation

$$n_0^2 = \left(1 + \frac{E_d}{E_0}\right) \tag{8}$$

The high-frequency dielectric constant $\varepsilon_\infty = n_0^2$ was calculated and presented in Table 2.

3.2.4. *High-frequency dielectric constant and carrier concentration*

The calculated value of the linear refractive index was used to obtain the high-frequency dielectric constant (ε_L) according to the relation [38]

$$\varepsilon_1 = n^2 = \varepsilon_L - \left(\frac{e^2 N}{4\pi^2 C^2 \varepsilon_0 m^*}\right)\lambda^2, \tag{9}$$

where ε_1 is the real part of dielectric constant, e is the charge of the electron, N is the free charge carrier concentration, ε_0 is the permittivity of free space, m^* is the effective mass of charge carrier, and c is the velocity of light. The intercept of the plot between n_2 vs λ^2 gives the value of ε_L and the value of N/m^* was obtained from the slope of the linear portion of straight-line fitting (Fig. 9). The ε_∞ increased from 8.05 to 8.11 with Ag deposition and to 8.59 for the $Te/As_{50}Se_{50}$ bilayer film. The ε_L was found to be 11.94 for $As_{50}Se_{50}$, 12.03 for $Ag/As_{50}Se_{50}$ and 12.37 for $Te/As_{50}Se_{50}$ thin film. The value of ε_L is more than that of ε_∞ is due to the increase in free charge carrier concentration [39].

3.3. Nonlinear optical susceptibility and nonlinear refractive index

The nonlinear optics is used to describe the phenomena that occur when the interactions occur between very high light intensities and the materials. The nonlinear optical quantities are internally connected with the nonlinear polarization and the incident energy [40]. The third-order harmonic generation, two-photon absorption and nonlinear refractive index (n_2) are evaluated from the third-order nonlinear optical susceptibility $\chi^{(3)}$ for nonlinear optical applications [41]. The linear refractive index is related to the linear optical susceptibility (χ^1) through the equation [42]

$$\chi^{(1)} = \frac{n^2 - 1}{4\pi} \tag{10}$$

Then, the relation between the linear susceptibility $\chi^{(1)}$ and nonlinear susceptibility $\chi^{(3)}$ involving an average energy gap (E_o) and single oscillator strength parameter (E_d) is given by generalized Miller's rule [43, 44]

Table 2 Optical parameters of the studied films

Sample	ε_∞	ε_L	$N/m^* \times 10^{46}$ (cm^{-3} eV^{-1})	$\chi^{(1)}$	$\chi^{(3)}$	n_2
$As_{50}Se_{50}$	8.06	11.94	4.22	0.562	16.95×10^{-12}	2.24×10^{-10}
$Ag/As_{50}Se_{50}$	8.12	12.08	4.08	0.567	17.57×10^{-12}	2.32×10^{-10}
$Te/As_{50}Se_{50}$	8.58	12.37	3.17	0.603	22.47×10^{-12}	2.88×10^{-10}

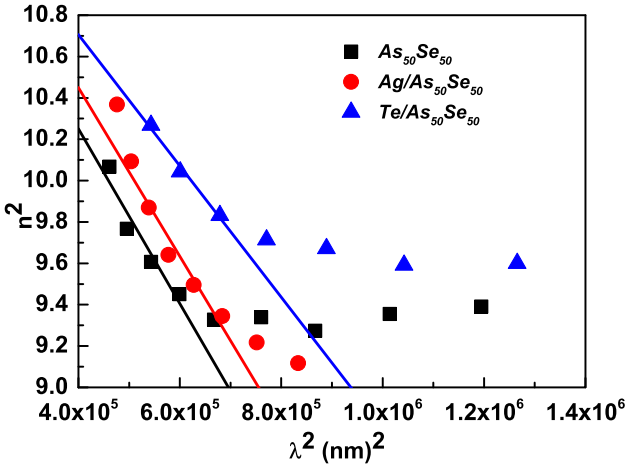

Fig. 9 n_2 versus ^{2} plot of $As_{50}Se_{50}$, $Ag/As_{50}Se_{50}$ and $Te/As_{50}Se_{50}$ thin films

$$\chi^{(3)} \cong A\left(\chi^{(1)}\right)^4, \tag{11}$$

where $A = 1.7 \times 10^{-10}$ (χ measured in esu) is an amount that is expected to be frequency independent and approximately the same for all materials.

In the long-wavelength limit ($h\nu \to 0$), the above equation becomes

$$\chi^{(1)} = \frac{n_0^2 - 1}{4\pi} \tag{12}$$

This makes Eq. 11 to the form

$$\chi^{(3)} \cong A\left[\frac{n_0^2 - 1}{4\pi}\right]^4 = A\left[\frac{E_0 E_d}{4\pi\left(E_0^2 - (h\vartheta)^2\right)}\right]^4 \tag{13}$$

The $\chi^{(1)}$ value for $As_{50}Se_{50}$, $Ag/As_{50}Se_{50}$ and $Te/As_{50}Se_{50}$ film are presented in Table 2. The $\chi^{(3)}$ values were calculated using Eq. 13, and it is observed that $\chi^{(3)}$ value is more for the $Te/As_{50}Se_{50}$ film than the $Ag/As_{50}Se_{50}$ film as presented in Table 2. The susceptibility increased monotonically with decreasing bandgap which is observed for the studied films as shown in Tables 1 and 2 like other studies [45–47]. The nonlinear refractive index is related to the third-order susceptibility $\chi^{(3)}$ by the relation [48]

$$n_2 = \frac{12\pi\chi^{(3)}}{n_0}, \tag{14}$$

where n_o is the static refractive index. The variation of n_2 follows the same trend as $\chi^{(3)}$.

The increase of E_d/E_o leads to an increase in the values of n_2 and $\chi^{(3)}$. The change in nonlinear parameters is very useful for UV nonlinear optical materials [49]. The deposition of Ag on the As_2Se_3 layer influences the optical parameters of the metal–chalcogenide (Ag/Se) interface due to the interaction among the elements as stated by Popescu et al. [50]. The large values of the nonlinear parameters for the Ag and Te deposited thin films are very important for the formation of low-power devices for nonlinear optical applications.

4. Conclusion

The thermally deposited thin films of $Ag/As_{50}Se_{50}$ and $Te/As_{50}Se_{50}$ undergo no structural change after deposition of Ag and Te onto $As_{50}Se_{50}$. The optical transmittance decreased, whereas the absorption coefficient increased for the bilayer thin films. The optical bandgap was found to be decreased with the increase in disorder as reflected from the $B^{1/2}$ and E_u values. The homopolar bonds that formed at the interface increased the density of defect states which decreased the bandgap. The linear and nonlinear refractive index was increased along with the increase in $\chi^{(3)}$. However, the change is more for the $Te/As_{50}Se_{50}$ film than that of $Ag/As_{50}Se_{50}$ film. The change in such optical constants can be used to design specific types of optoelectronic and integrated optical elements, which need high local changes of optical parameters.

Acknowledgements The author Dr. Naik thank ICT-IOCB for the Start-up Research grant and the Department of Physics, Indian Institute of Science (IISc.) for optical measurements.

References

[1] M P Abubacker, G Selvan and A R Balu *J. Mater Sci: Mater Electron* **28** 10433 (2017)

[2] V S Shiryaev et al. *J. Non-Cryst. Solids* **448** 11 (2016)
[3] J Sharma et al. *J. Alloys Compd*. **724** 62 (2017)
[4] R Kaur et al. *Superlatt. Microstruct*. **98** 187 (2016)
[5] T Wagner, S Schroeter, T Glaser and M Vlcek J. *Non-Cryst. Solids* **326–327** 500 (2003)
[6] V Takats, A C Miller, H Jain, A Kovalsky and S Kokenysi *Thin Solid Films* **519** 3437 (2011)
[7] M Behera and R Naik *Appl. Phy. A* **122** 913 (2016)
[8] M Behera, S Behera and R Naik *RSC Adv.* **7** 18428 (2017)
[9] K Suzuki, Y Hamachi and T Baba *Opt. Exp*. **17(25)** 22393 (2009)
[10] R Naik, M Behera, A Aparimita and R Panda *AIP Conf. Proc*. **2005** 060001 (2018)
[11] P Yadav and A Sharma *J. Elect. Mater*. **44(3)** 916 (2015)
[12] D Cotter et al. *Science* **286** 1523 (1999)
[13] M B Pushkarsky, M E Webber, T Macdonald and C K N Patel *Appl. Phys. Lett*. **88** 044103 (2006)
[14] B Jalali *Nat. Photonics* **4** 506 (2010)
[15] H Nasu, K Kubodera, H Kobayashi, M Nakamura and K Kamiya *J. Am. Ceram. Soc*. **73** 1794 (1990)
[16] I D Tolmachov and A V Stronski *J. Quantum Electron. Optoelectron*. **13** 276 (2010)
[17] E V Lyubin, M Klebanov, I Bar, N P Eisenberg, and M Manevich *J. Vac. Sci. Technol. B* **15** 823 (1997)
[18] C Quemard, F Smektala, V Couderc, A Barthelemy and J Lucas *J. Phys. Chem. Solids* **62** 1435 (2001)
[19] E M Vogel, M J Weber and D M Krol *Physics. Chem. Glasses* **32** 251 (1991)
[20] H C. Nguyen et al. *Appl. Phys. Lett*. **92** 101127 (2008)
[21] A A Abuelwafa et al. *Opt. Mat.* **49** 271 (2015)
[22] A V Kolobov and S R Elliot *Adv. Phys*. **40** 625 (1991)
[23] A Herzi, M Sebais, B. Boudine, O Halimi, B Rahal and L Guerbous *Acta Phys. Polonica A* **135(3)** 526 (2019)
[24] P Pradhan, R Naik, N Das and A K Panda *Opt. Mater.***75** 699 (2018)
[25] K Seedek et al. *J. Phys. D: Appl. Phys*. **27** 156 (1994)
[26] R Naik, A K Behera, A Aparimita, C Sripan and R Ganesan *Phase Tran*. **92** 683 (2019)
[27] J Tauc *Amorphous and Liquid Semiconductor*, (Plennum Press, New York, 1974) p 179
[28] S A Yamini, V Patterson and R Santos *ACS Omega* **2** 3417 (2017)
[29] N F Mott and E A Davis, *Electronics Processes in Non-crystalline Materials* (Clarendon, Oxford, 1979) p 428
[30] M Behera, R Panda and R Naik *Ind. J. Phys.* **91(5)** 555 (2017)
[31] F Urbach *Phys. Rev*. **92** 1324 (1953)
[32] H E Atyia and N A Hageb *Optik* **127** 3888 (2016)
[33] R Naik, S Jena, R Ganesan and N K Sahoo *Ind. J. Phys*. **89** 1031(2015)
[34] R Swanepoel *J.Phys. E Sci. Instrum*. **16** 1214 (1983)
[35] R Naik, C Sripan and R Ganesan *Opt. Laser Technol*. **90** 158 (2017)
[36] P Knotek et al. *Mater. Chem. Phys*. **119** 315 (2010)
[37] S H Wemple and M DiDomenico *Phys. Rev. B*. **3** 1338 (1971)
[38] M Behera et al. *Curr. Appl. Phys.***19(8)** 884 (2019).
[39] M M El-Nahass, M H Ali and I T Zedan *J. Non-Cryst. Solids* **404** 78 (2014)
[40] R Naik, A Aparimita, D Alagarasan, S Varadharajaperumal and R Ganesan *Opt. Quant. Elect.* **52** 136 (2020)
[41] M Dongol, A F Elhady, M S Ebied and A A Abuelwafa *Opt. Mater*. **78** 266 (2018)
[42] H M Alsoghier et al. *J. Mol. Struct*. **1179** 315 (2019)
[43] J J Wayne *Phys. Rev. B* **178** 1295 (1969)
[44] A A Abuelwafa, M S Abd El-Sadek and I S Yahia *Opt. Laser. Techn*. **108** 241 (2018)
[45] I Sharma, S K Tripathi and P B Barman *J. Appl. Phys.* **110** 043108 (2011)
[46] S Y Kim, M Kang and S Y Choi *Thin Solid films* **493** 207 (2005)
[47] R Naik, A Aparimita, C Sripan and R Ganesan *Optik* **194** 162894 (2019)
[48] M Dongol, A F Elhady, M S Ebied and A A Abuelwafa, *Ind. J. Phys*. (2020) https://doi.org/10.1007/s12648-020-01787-3
[49] X Dong et al. *Chem. Commun*. **54** 5792 (2018)
[50] M Popescu, F Sava and A Loeinczi *J. Opto. Electron. Adv. Mat.* **11** 1586 (2009)